ROWAN UNIVERSITY **2014**

Validation of SF-CIHT Technology

Valuator:
K.V. Ramanujachary
Professor
Department of Chemistry and Biochemistry
Rowan University, Glassboro, NJ, 08028

Submitted to
BlackLight Power, Inc.

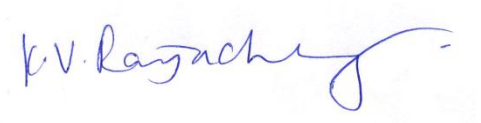

Evaluator's Signature: Date: February 2014

BLACKLIGHT POWER (BLP) SF-CIHT CELL VALIDATION (February 2014)

The present report deals with validation studies of SF-CIHT (Solid-Fuel-Catalyst-Induced-Hydrino-Transition) cells that were assembled and tested at BlackLight Power, Inc. at their Cranbury, NJ laboratories. By applying a high current to solid fuels, BLP has achieved a breakthrough in power and power density. Using earth-abundant and eco-friendly chemicals, explosive power of millions of watts and astonishing tens of billions of watts per liter were demonstrated. Using existing components and technologies, systems could be engineered and built into very inexpensive commercial power generators that use H_2O as fuel having 100 times the volumetric energy content of gasoline.

A. Ignition of H_2O-based solid Fuels with a Low Voltage, High Current

Controls and test samples each comprising solid fuel encased in Al or as pellets were confined between RWMA class 2 copper/C18200 alloy electrodes rods (0.6 to 1.2% Cr, 5/8" OD) of a commercial spot welder (Acme Electric Welder Company model 3-42-75, 75 KVA with Warren control, Model 108) and exposed to the high current (10,000-30,000 A). The electrodes were replaced between samples. The voltage was measured by a data acquisition system (DAS), and the current was measured with a Rogowski coil (Additional details are given in Sec. B). The baseline waveform of 6 V RMS of the high-current source (Figure 1) was recorded using a control nickel sheet sample. As seen in the figure, the event lasts roughly 30 ms. During the control test, the current voltage stays within the +/- 8V bounds but shows interruptions at times due to the welder controller that shorts the power at controlled intervals to control the energy delivered to the sample. The current follows a regular AC curve (with the exception of a short interruption at 5 ms after contact). The peak current is roughly 27 kA. For the control run, the time integral of VI yields 2067 J.

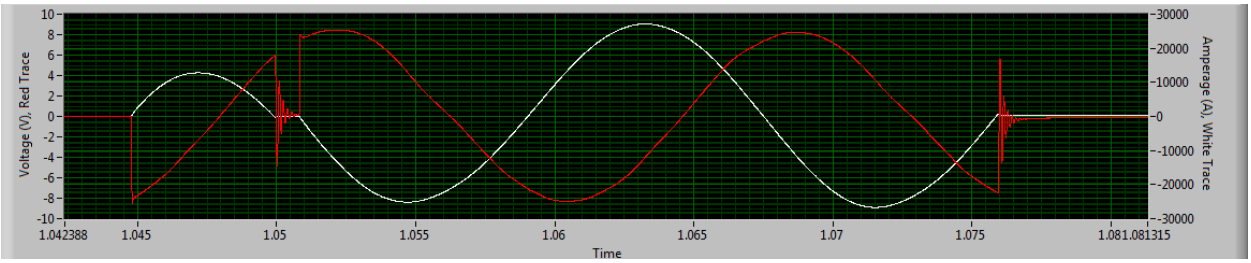

Figure 1: Nickel sheet control on the instrumented spot welder.

In addition to the nickel sheet control, eight tests were run, and the conditions were as follows:
Controls:

1) A gold 0.010” diameter wire
2) Setaram 30 microliter Aluminum crucible. Empty.
3) A pressed silver pellet with no additives

Solid Fuel Tests

4) Crucible with 30 mg deionized water
5) Crucible with Cu, CuO, and 15 mg water mixed
6) Crucible with 30 mg water and large mesh copper (100 mg)
7) A silver pellet with $MgCl_2$ and 30 μl water, pressed.
8) A repeat of test 7 with the sample prepared immediately before the run.

Only heating alone or heating with melting was observed for all of the controls in addition to the nickel sheet. In contrast, all of the H_2O-based solid fuels underwent a detonation event with a loud blast, bright light emission, and a pressure shock wave. The sample appeared to have been completely vaporized and atomized to form what appeared to be an ionized supersonically expanding plasma that was confirmed with a high-speed camera (6500 frames per second) provided by BLP as shown in Figure 2. The operating voltage was 6 volts RMS (60 Hz AC), though some voltage deviations were observed during the actual initiation event due to power-wave reflection from the circuit interruption by the high pressure of the blast following the initiation.

Figure 2: Supersonic expanding plasma formed from the high-current detonation of the solid fuel Cu + CuO + H_2O filmed at 6500 frames per second.

Control tests (Tests 1, 2, and 3) produced no appreciable acoustic or light-emitting event. Traces were similar to the nickel sheet control test. In the wire test, no wire explosion or disruption in conductivity was observed. It simply glowed red and exhibited some melting. The current/voltage trace from test 3 is shown below:

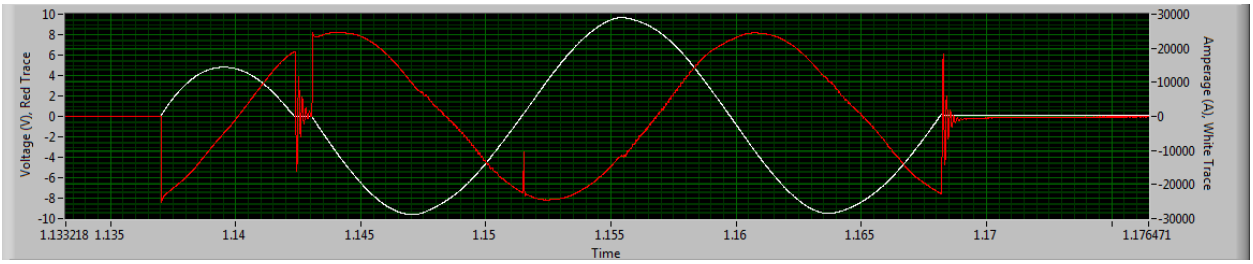

Figure 3: Traces from the test using a silver control pellet.

This trace is very similar in all aspects to the nickel control with a time-integrated power of 2109 J. Tests in which there was water vapor present showed significantly different behavior, both qualitatively and quantitatively. Tests were accompanied by a blast having a shock wave that was similar to those observed in high explosives. In addition, there was typically a fairly bright flash of light from supersonically expanding plasma. The current/voltage traces were also significantly different. For example, test 7 (for which test 3 served as the control) is shown in Figure 4 below wherein the time-integrated power was 1888 J.

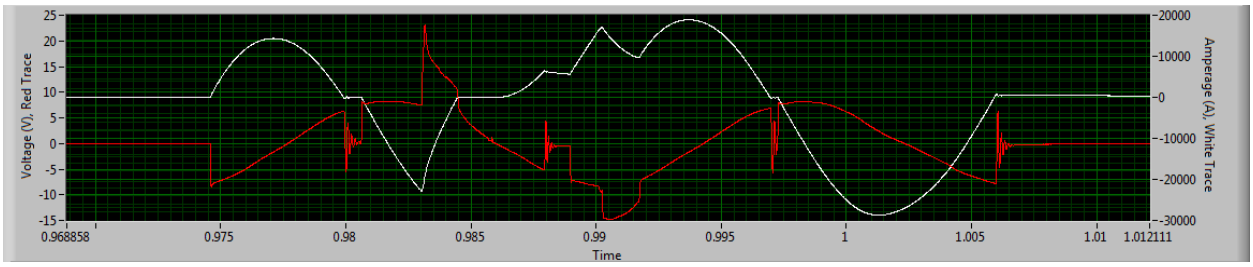

Figure 4: The current and voltage traces for Test 7 (Silver/$MgCl_2$/H_2O).

The event duration was the same in the control and test cases and was set by the power source. However, there were much larger and more numerous distortions of the otherwise AC waveform. This effect was especially pronounced for the current trace, which showed only minor deviation from a sinusoidal profile in the control experiments. In contrast, the current exceeded 28,000 A at peak. The voltage trace also spiked well outside its +/-6V envelope, reaching above 20 volts at one point due to power-wave reflections with mechanical disruptions of the power-flow from the pressure of the ensuing detonation of the H_2O-based solid fuel. Similar traces were observed for all reactive tests (Tests 4-8). But, there were qualitative differences in the output from the tests. For instance, test 5 was louder than test 7. However, these observations were difficult to quantify. Electrodes were generally observed to be heavily pitted after a reactive test, with pits perhaps one or two mm in diameter, and typically just under 1 mm deep. Similar results for identical active tests run under an argon atmosphere were reported by BLP.

X-ray diffraction was performed on the starting materials and the solid fuel Ag + $MgCl_2$ + H_2O as it was prepared during validation and then detonated. The results follow:

$MgCl_2$ Starting Material:

Major:	$MgCl_2$ (>1,000 Å)
Minor:	$MgCl_2 \cdot 4H_2O$ (513Å)
	$MgCl_2 \cdot H_2O$ (836Å)

Ag Starting Material:

Ag	100% (446Å)

Solid Fuel:

Ag	75.2 ± 1.1% (434 Å)
$MgCl_2(H_2O)_6$	24.8 ± 1.3% (>1,000 Å)

B. Calorimetry of Solid Fuel of the SF-CIHT Cell

Calorimetry was performed on two solid fuel pellets and a control Ni sheet using a Parr 1341 plain-jacketed calorimeter with a Parr 6775A calorimeter thermometer interfaced with a computer. A Parr 1108 oxygen combustion chamber of the calorimeter was modified to permit initiation of the chemical reaction with high current. Copper rod ignition electrodes that comprised 1/2" outer diameter (OD) by 12" length copper cylinders were fed through the sealed chamber containing a nickel sheet as a control resistive load for calibration of the heat capacity of the calorimeter or a solid fuel pellet wherein the ends had a copper clamp that tightly confined each sample. The calorimeter water bath was loaded with 2,000 g DI water (as per Parr manual). The power source for calibration and ignition of the solid fuel pellet was a Taylor-Winfield model ND-24-75 spot welder that supplied a short burst of electrical energy in the form of a 60 Hz low-voltage of about 8 V RMS and high-current of about 15,000 to 20,000 A. The power applied was somewhat lower in the calorimetry runs to increase the energy gain. Control detonation experiments were also run at this power level to compare the relative extent of detonation of the sample in the calorimeter cell versus that observed using the spot welder electrodes directly wherein the power loss was less. The input energy of the calibration and ignition of the solid fuel was given as the product of the voltage and current integrated over the time of the input. The voltage was measured by a data acquisition system (DAS) comprising a PC with a National Instruments USB-6210 data acquisition module and Labview VI. The current was also measured by the same DAS using a Rogowski coil (Model CWT600LF with a 700 mm cable) that was accurate to 0.3% as the signal source. V and I input data was obtained at 10 KS/s and a voltage attenuator was used to bring analog input voltage to within the +/-10V range of the USB-6210.

The prior calibrated heat capacity of the calorimeter and electrode apparatus used to measure the energy balance of solid fuel samples was 12,800 J/°C. A first sample of solid fuel comprising Cu (35.5 mg) + CuO (44.5 mg) + H_2O (30 mg) that was sealed in an aluminum DSC pan (70 mg) (Aluminum crucible 30 µl, D:6.7x3 (Setaram, S08/HBB37408) and Aluminum cover D: 6,7, stamped, tight (Setaram, S08/HBB37409)) was ignited with an applied peak 60 Hz voltage of 3.5 V and a peak current of about 20,000 A. The input energy measured from the voltage and current over time was 180 J to ignite the sample as indicated by a disruption spike in the waveforms with a total of 890 J input by the power pulse of the spot welder (Figure 5), and the total output energy calculated for the calorimetry thermal response to the energy released from the ignited solid fuel using the calibrated heat capacity was 1380.88 J (Figure 6). By subtracting the input energy, the net energy was 490.88 J for the 0.110 g sample. In control experiments with H_2O, the alumina pan did not undergo a reaction other than become vaporized

in the blast. XRD also showed no aluminum oxide formation. Thus, the theoretical chemical reaction energy was zero, and the solid fuel produced 4462 J/g of excess energy presumably due to the formation of a special state of hydrogen. The energy gain relative to the input energy to detonation was 490.88/180 = 2.73. A major portion of the input energy is attributed to the melting of the Al crucible that is not necessary. For example, a 1 cm^2 nickel screen conductor coated with a thin (<1 mm thick) tape cast coating of NiOOH, 11 wt % carbon, and 27 wt% Ni powder was detonated with a 5 J input energy (Figure 7). A thermodynamic calculation of the energy to vaporize only the 350 mg of NiOOH and 50 mg of Ni metal of the sample showed an energy release of 3.22 kJ.

Figure 5. The voltage and current (top), power and energy (middle), and absolute voltage and absolute current (bottom). The detonation is indicated by the disruption of the waveform. The detonation occurs at 180 J input energy, about 20% of the total input energy.

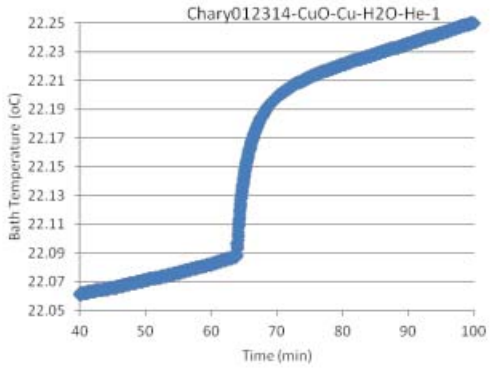

Fuel: 80mg CuO+Cu (1:1); 30mg H2O.
Assembly: S30-Al Pan, upright, Flat, He
Spot Welder: Tap 8, ST1, HeatT2, Pulse1, HoldT1, PC1, 100%
Note: Dr. Chary Validation

Parr	
Chary012314-CuO-Cu-H2O-He-1	
Total Temp Rise (oC)	0.132
60% Temp Rise	0.0792
Temp of 60% T Rise, Tb	22.1662
Time of 60% T Rise, b	60.033
Firing Temp, Ta	22.087
Firing Time, a	63.783
Heat End Temp, Tc	22.219
Heat End Time, c	78.817
r1	0.001331875
r2	0.001549907
dT=Tc-Ta-r1*(b-a)-r2*(c-b)	0.107881078
Cp	12800
Eout =Cp*dT (J)	**1380.88**
Ein (J)	**890.00**
dE (J)	**490.88**

Figure 6. First validation test of solid fuel CuO + Cu + H_2O.

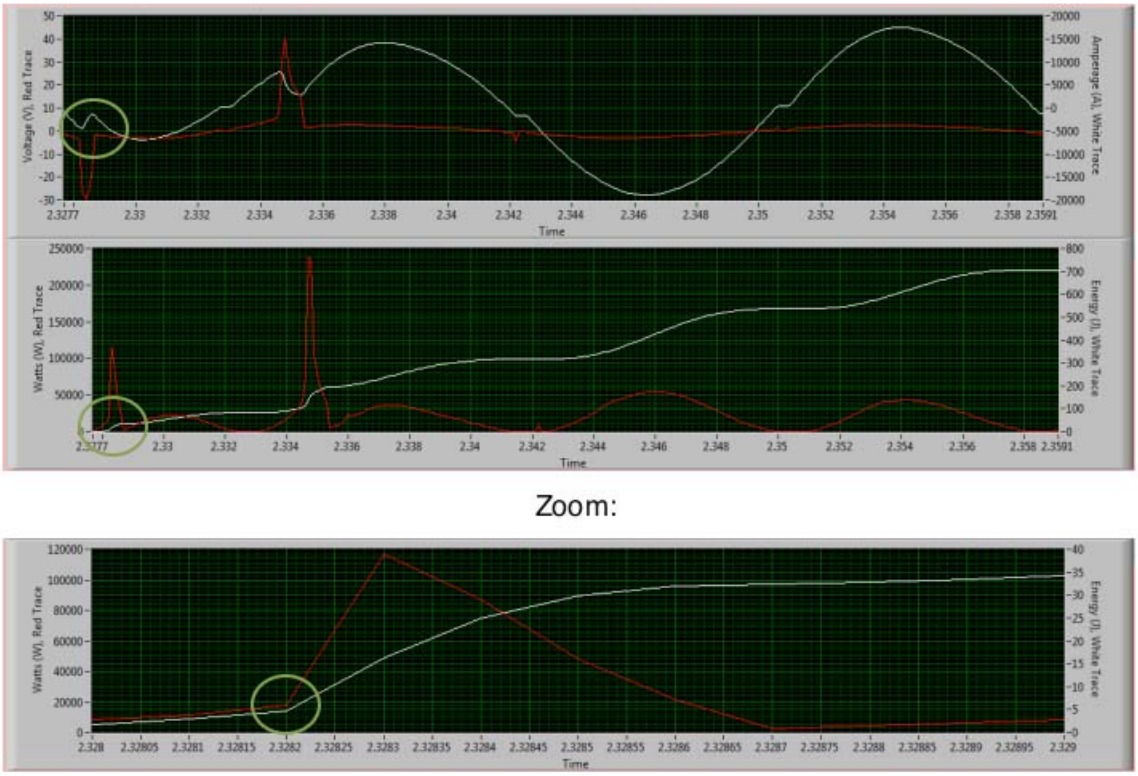

Figure 7. The voltage and current (top), power and energy (middle), and expansion of the power and energy traces (bottom). The detonation is indicated by the disruption of the waveform. The detonation occurs at 5 J input energy, less than 1% of the total input energy and 1% of the output energy.

A second sample of solid fuel comprising Cu (63 mg) + CuO (40 mg) + H_2O (30 mg) that was sealed in the aluminum DSC pan (70 mg) was ignited with an applied peak 60 Hz voltage of 3.1 V and a peak current of about 19,000 A. The input energy measured from the voltage and current over time was 232 J to ignite the sample as indicated by a disruption spike in the waveforms with a total of 879 J input by the power pulse of the spot welder, and the total output energy calculated for the calorimetry thermal response to the energy released from the ignited solid fuel using the calibrated heat capacity was 1352.67 J (Figure 8). By subtracting the input energy, the net energy was 473.67 J for the 0.133 g sample. The solid fuel produced 3561 J/g of excess energy in the formation of new state of hydrogen. The energy gain relative to the input energy to detonation was 473.67/232 = 2.04.

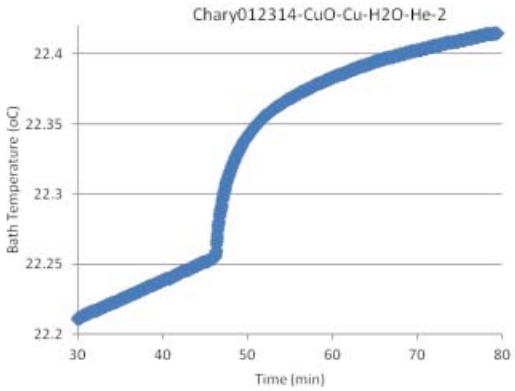

Fuel: 40mg CuO; 63mg Cu; 30mg H2O.
Assembly: S30-Al Pan, upright, Flat, He
Spot Welder: Tap 8, ST1, HeatT2, Pulse1, HoldT1, PC1, 100%
Note: Dr. Chary Validation

Parr	
Chary012314-CuO-Cu-H2O-He-2	
Total Temp Rise (oC)	0.141
60% Temp Rise	0.0846
Temp of 60% T Rise, Tb	22.3396
Time of 60% T Rise, b	49.833
Firing Temp, Ta	22.255
Firing Time, a	46.067
Heat End Temp, Tc	22.396
Heat End Time, c	65.55
r1	0.002715901
r2	0.001596638
dT=Tc-Ta-r1*(b-a)-r2*(c-b)	0.105677557
Cp	12800
Eout =Cp*dT (J)	**1352.67**
Ein (J)	**879.00**
dE (J)	**473.67**

Figure 8. Second validation test of solid fuel CuO + Cu + H_2O.

The nickel sheet control data are shown in Figure 9. For this test, the integrated VI over the waveform duration was 882.00 Joules of energy to the sample. The output calculated from the easily resolvable temperature rise of 0.083 °C and the prior determined heat capacity was 911.47 J. The net was only 29.47 J from the expected value of zero net energy and the gain was only 1.03, demonstrating that the prior determined heat capacity was within experimental error.

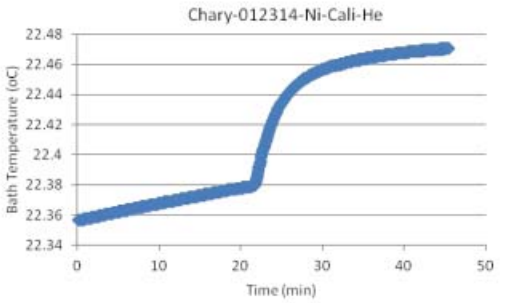

Fuel: N/A
Assembly: 2x 0.02" Ni strip, upright, Flat, He
Spot Welder: Tap 8, ST1, HeatT2, Pulse1, HoldT1, PC1, 100%
Note: Dr. Chary Validation, Ni control

Parr Calibration	
Chary-012314-Ni-Cali-He	
Total Temp Rise (oC)	0.083
60% Temp Rise	0.0498
Temp of 60% T Rise, Tb	22.4298
Time of 60% T Rise, b	24.5
Firing Temp, Ta	22.38
Firing Time, a	21.533
Heat End Temp, Tc	22.463
Heat End Time, c	34.533
r1	0.001052
r2	0.000864183
dT=Tc-Ta-r1*(b-a)-r2*(c-b)	0.07120837
Ein	**882.00**
Cp = Ein/dT	**12386.18**

Parr	
Chary-012314-Ni-Cali-He	
Total Temp Rise (oC)	0.083
60% Temp Rise	0.0498
Temp of 60% T Rise, Tb	22.4298
Time of 60% T Rise, b	24.5
Firing Temp, Ta	22.38
Firing Time, a	21.533
Heat End Temp, Tc	22.463
Heat End Time, c	34.533
r1	0.001052
r2	0.000864183
dT=Tc-Ta-r1*(b-a)-r2*(c-b)	0.07120837
Cp	12800
Eout =Cp*dT (J)	**911.47**
Ein (J)	**882.00**
dE (J)	**29.47**
Eout/Ein	**1.03**

Figure 9. Nickel sheet control run.

C. Differential Scanning Calorimetry (DSC) of Solid Fuels

A BLP solid fuel (4.7 mg $Cu(OH)_2$ + 11.8 mg $FeBr_2$) capable of a hydroxide-halide exchange reaction to form HOH and H necessary to the proposed BLP hydrino reaction were tested for excess energy over the maximum theoretical using a Setaram DSC 131 differential scanning calorimeter with Au-coated crucibles. For all tests, the fuel samples that I assisted in preparing were loaded into crucibles in an argon glove box. The loaded crucibles were mounted into the DSC instrument and initially equilibrated at 30 °C for 20 min. The solid fuel test was heated from 30 °C to 280 °C at the rate of 10 °C/min, cooled from 280 °C to 30 °C at 10 °C/min, and finally equilibrated at 30 °C for 20 min. The control was run the same over the temperature range of 30 °C to 280 °C. Analysis was performed using the Setaram software wherein the DSC (Setaram DSC131) calibration for enthalpy and temperature was confirmed by using 16.6 g of pure indium that served as a standard for the melting point and enthalpy of melting. As shown in Figure 10, the observed T_m onset was 150.12 °C and ΔH was 29.41 J/g compared to the standard values of T_m onset of 156.60 °C and ΔH of 28.51 J/g.

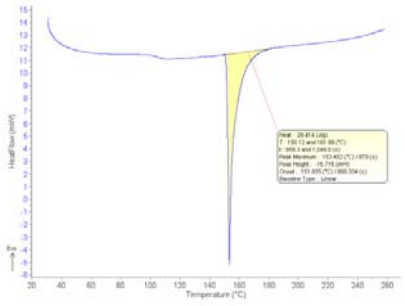

Figure 10. Indium metal, DSC heating trace.

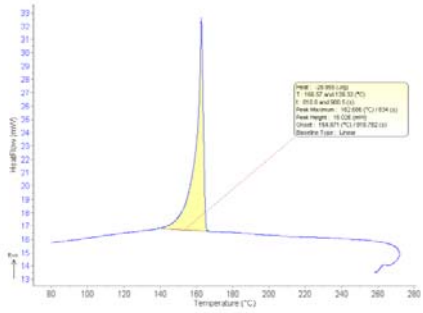

Figure 11. Indium metal, DSC cooling trace.

For the solid fuel test (Figure 12), a prominent exotherm was observed upon heating between 110 and 260 °C, and a very small exotherm was observed during cooling wherein the total energy was -190.3 J/g compared to a maximum theoretical energy of -60.38 J/g. The theoretical reactions and a summary of the energy balance are given in Table 1. The large energy release cannot be explained by conventional chemistry; the results being 313% that of the maximum theoretical energy possible.

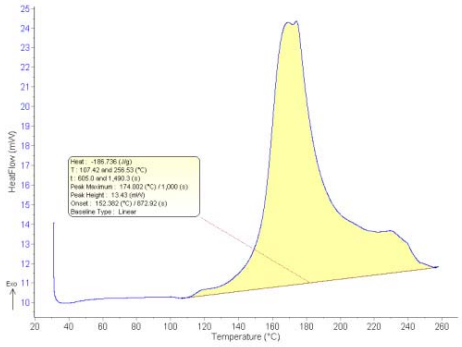

Figure 12. $Cu(OH)_2 + FeBr_2$, DSC heating trace.

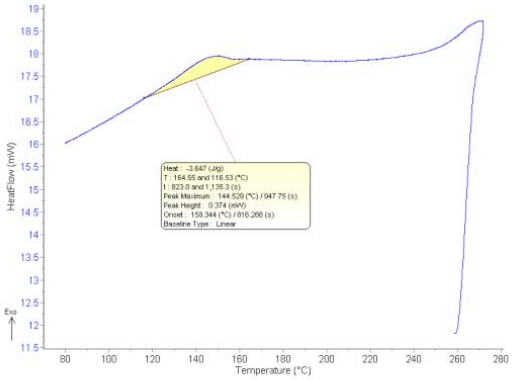

Figure 13. $Cu(OH)_2 + FeBr_2$, DSC cooling trace.

012314Chary-validation, Cu(OH)2 + FeBr2

Reactant	FeBr2.	Cu(OH)2	ΔE, J/g	Excess energy, J/g	Energy Gain
quantity, mg	11.80	4.70	-190.38	-129.56	3.13
quantity, mmol	0.0547	0.0482			
HOF, dH (KJ/mol)	-249.80	-450.00			

Product	Fe(OH)2	CuBr2	Fe2O3	FeBr2.2H2O	CuBr	Cu2O	FeO	H2O	HBr (g)
HOF, dH (KJ/mol)	-574.00	-141.80	-822.20	-861.40	-104.60	-168.60	-272.00	-285.80	-36.30

Assumed Reaction I	Energy, kJ/reaction	FeBr2 used, mmol	Cu(OH)2 used, mmol	Cu(OH)2 left, mmol	FeBr2 left, mmol	Energy out, J	theoretical energy, J/g
Cu(OH)2 + FeBr2 = Fe(OH)2 + CuBr2	-16.00	0.0482	0.0482	0.0000	0.0065	-0.77	-46.74
10Cu(OH)2+9FeBr2 = 2Fe2O3+5FeBr2.2H2O+8CuBr+Cu2O+3/2 O2	-208.20	0.0434	0.0482	0.0000	0.0113	-1.00	-60.83
3Cu(OH)2 + 3FeBr2 = Fe2O3 + FeO + 3CuBr + 2H2O + 2HBr + 1/2 Br2	47.40	0.0482	0.0482			0.76	

Table 1. Theoretical calculations of the heat generated by conventional reactions of each reactant and the mixture of $Cu(OH)_2$ + $FeBr_2$.

D. 10 MW Generator System Design

Using the observed parameters of these validation tests, I can make an assessment of the commercial feasibility of a power generator based on the BlackLight Power, Inc. SF-CIHT cell. The solid fuel such as Cu + CuO + H_2O comprises cheap, abundant, nontoxic, commodity chemicals, with no apparent long-term supply issues that might preclude commercial, high volume manufacturing. Based on regeneration tests by BLP, only H_2O need be added back; so, long term operation using H_2O as the only consumable is expected. The ignition test confirmed that a very powerful supersonic expanding plasma was formed of extraordinary power and power density that can be quantified. The energy released from 10 μl of solid fuel was measured to be about 500 J. Based on the energy to vaporize the fuel and form the plasma, the energy release is much higher. Less was observed in the calorimeter since a good fraction of the voltage and current are dissipated in the 1/2" leads before the power was flowed through the fuel. Consequently, the ignition was not complete. This was confirmed by the observation that the fuel was completely vaporized in the detonation experiments; whereas, about one half remained after being ignited in the bomb calorimeter cell. The time of the denotation event corresponding

to the time of the energy release was maximally given by the mechanical response time of 1 ms noted by the waveform disruption event; however, based on the high speed photography that BLP recorded on the plasma, the blast time is more likely about 10 μs. Then, the power can be conservatively given by dividing the energy of 500 J by the event time of 1 ms, resulting in 500 kW. The upper bound is more like 1 kJ divided by 10 μs giving 100 MW. The volume of the fuel was 10 μl; so, the corresponding power density was in the range of 50 GW/liter to 10 TW/liter. These are unprecedented considering that the highest controllable power density is the 10 kW/liter of an internal combustion engine. The SF-CIHT cell's power density is at least five million times higher. This should have profound ramifications regarding the future of power.

BLP performed analytical tests on solid fuel detonation products and EUV spectroscopy on the exploded solid fuel. The analytical results are consistent with a model in which the product was $H_2(1/4)$ having a total energy of sixteen times that of H_2. Soft X-ray continuum radiation observed in these experiments tie well with a transition of the electron of H to H(1/4), an energy level sixteen times below the 13.6 eV level of H. These results confirm that BLP's power-producing system catalytically converts the hydrogen of the H_2O-based solid fuel into a non-polluting product, comprising lower-energy state hydrogen wherein the energy release of H_2O fuel is 100 times that of an equivalent amount of high-octane gasoline.

BLP has developed a system engineering design of an electric generator that is closed except for the addition of H_2O fuel and generates 10 MW of electricity, enough to power ten thousand homes. According to BLP's design (Figures 14A-C), each SF-CIHT cell comprises two electrodes that confine a highly electrically conductive H_2O-based solid fuel that serves as a source of reactants to form the low-energy state of hydrogen. A low-voltage, very high current (about one thousand times that of household currents) ignites the water to generate a burst of plasma power packed with millions of watts that can be directly converted to electricity using proven plasma to electric power conversion technology such as a magnetohydrodynamic or plasmadynamic converter. A magnetohydrodynamic (MHD) converter is an electrical generator that uses no moving parts. It comprises a magnet as in a conventional generator, but the conductor that moves in this case is the flowing plasma that produces a voltage at a pair of electrodes that are perpendicular to both the direction of plasma flow and the magnetic field of the magnet.

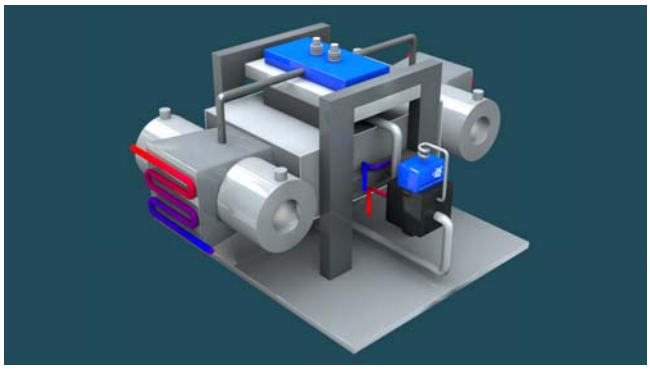

(A)

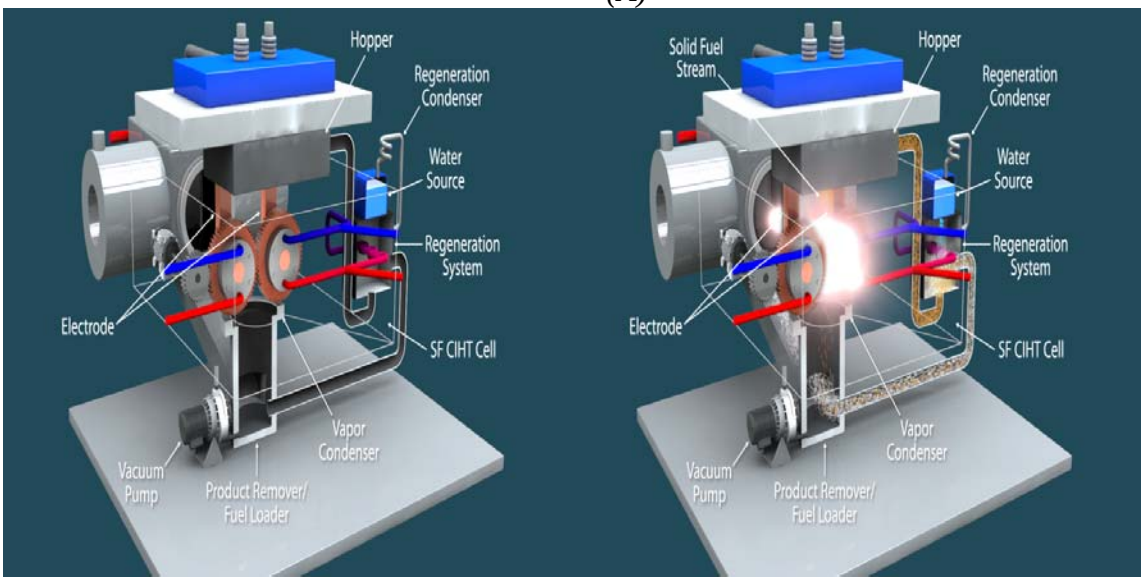

(B) *(C)*

Figures 14A-C. System design of 10 MW SF-CIHT generator.

In an embodiment, a 10 MW power generator undergoes the following steps:

1. Fuel flows from the hopper into a pair of gears that confines about 0.5 g aliquots of highly conducting solid fuel in the interdigitating regions wherein a low voltage, high current is flowed through the fuel to cause it to ignite. The ignition releases about 10 kJ of energy per aliquot. The gears comprise 60 teeth and rotate at 1000 RPM such that the firing rate is 1 k Hz corresponding to 10 MW of power.
2. An essentially fully ionized plasma expands out from the gears on the axis perpendicular to the gears and enters the magnetohydrodynamic or plasmadynamic converter wherein the supersonic plasma flow is converted to electricity.

3. A portion of the electricity powers the source of electrical power to the electrodes and the rest can be supplied to an external load following power conditioning by the corresponding unit. Heat that is removed from the gear hub by an electrode heat exchanger flows to a regeneration system heat exchanger, and the rest flows to an external heat load.
4. The plasma gas condenses to product comprising the solid fuel without H_2O.
5. An auger such as one used in the pharmaceutical or food industries transports the product powder to a regeneration system wherein it is rehydrated with steam wherein the steam is formed by flowing H_2O from a H_2O reservoir over the hot coils of the regeneration system heat exchanger.
6. The regenerated solid fuel is transported to the hopper by an auger to permit the continuous use of the fuel with H_2O add back only.

The gear dimensions are quite small for the power output. Assume 0.5 gram of solid fuel yields 1 kJ of energy. Assuming that the density of the fuel is the density of Cu, 8.96 g/cm^3, then the volume of fuel per tooth in the interdigitating area is 0.056 cm^3. If the conduction depth is 2 mm to achieve high conductivity through the fuel, then the fuel base defined by the interdigitation gap of the triangular teeth of each gear is 4 mm, and the gear width is 0.11 cm^3/(0.2cm)(0.4cm) = 1.39 cm. Remarkably, the concept device is less than a cubic foot in volume.

All of the parts of the SF-CIHT power generator comprise existing technology. To arrive at a cost estimate, consider a very conservative cost of the magnets of four times $10,000 a piece; $2000 for a stainless steel reactor vessel, solid fuel hopper, and regenerator chamber; $3000 for augers; $3000 for power supplies and control electronics; $1000 for the vacuum pump and gear drive motor, and $2000 for the ignition gears, bus bars, an heat exchangers. The total cost is well under $100,000. 10 MW is equivalent to 10,000 kW; so, the cost should be well under $10/kW compared to over one hundred times that for conventional power sources of electricity.

SF-CIHT power would be available anytime and independent from existing infrastructure such as the grid and fuels in the case of electricity, and fuels in the case of motive power. Applications and markets for the SF-CIHT cell extend across the global power spectrum, including thermal, stationary electrical power, motive, and defense.